



RESIDUAL DISPLACEMENTS IN CAPACITY DESIGNED REINFORCED CONCRETE STRUCTURES

Alessandro DAZIO¹

SUMMARY

Large-scale tests on reinforced concrete walls and bridge piers performed at the Swiss Federal Institute of Technology (ETH), Zurich and at the University of California, San Diego (UCSD) confirmed that using capacity design principles the inelastic deformation capacity of reinforced concrete structure can be greatly improved. However, the tests clearly indicated residual permanent deformations as possibly the major drawback of ductile structures. Structural elements with a high value of the new design parameter α_n , defined as the ratio between the bending strength of the element due to axial load only and its total bending strength, showed much lower permanent deformations upon unloading. The hysteretic behavior of such elements substantially differed from the commonly used elasto-plastic or Takeda-type hysteretic models, i.e. showing a reduced energy dissipation capacity and different stiffness degradation. These differences raised questions on the applicability of commonly used design tools like the equivalent force method, the capacity spectrum method or the direct-displacement design to the design of such structures. To answer these questions a fiber-element, able to carefully predict the behavior of structural elements with different values of α_n was developed and checked against experimental evidence. Subsequently, an extensive parametric study using nonlinear time-history analyses was performed, showing that elements with a high value of α_n had a larger ductility demand only at very high ductilities, making the use of such element extremely appealing in performance based design. The paper presents the conducted large-scale tests, the developed fiber-element, and the results of the performed time-history analyses. In conclusion recommendations on the optimum value of α_n are given and strategies to reduce permanent deformation are outlined both for buildings and bridge piers. In the latter case presenting as an example the West Anchor Pier of the New San Francisco-Oakland Bay Bridge.

INTRODUCTION

Reinforced concrete (RC) structural wall buildings are popular in Switzerland and Central Europe. Such buildings, as shown in Figure 1a, are often conceived as structural wall systems consisting of flat slabs, columns designed for gravity loads only and RC structural walls. Flat slabs are beamless concrete slabs typically with spans of 6 to 9m and thickness of 20 to 30cm, which are often strengthened around columns to prevent punching shear failure. Columns are in most cases monolithic with the slabs and have a small cross section with typical dimensions ranging from 20 to 40cm designed to carry axial forces. Structural walls are relatively slender reinforced concrete walls fixed in a very stiff RC foundation box structure with one or more basement stories. The structural walls have to resist horizontal wind and earthquake forces

¹ Institute of Structural Engineering (IBK). Swiss Federal Institute of Technology (ETH), Zurich.

and, by means of capacity design principles, they can be designed to behave in a ductile manner. A lot of research on the behavior of ductile reinforced walls has been conducted all over the world. However, in Switzerland and in other regions of Central Europe the conceptual design and the construction methodologies, the ratio between seismic inertia forces and gravity loads and especially the mechanical properties of the reinforcing steel are quite different as in countries like New Zealand, USA and Japan. For this reason research results gained in these countries with high seismicity cannot be simply applied to Central Europe; they have to be adapted. To reach this goal and to give the practising structural designer recommendations to design better structural wall systems, several reinforced concrete walls were tested by Dazio, Lestuzzi and Thiele at the Swiss Federal Institute of Technology [1-3].

In the following sections some of the test results are briefly presented and selected basic aspects of the behavior of reinforced concrete structural walls are discussed.

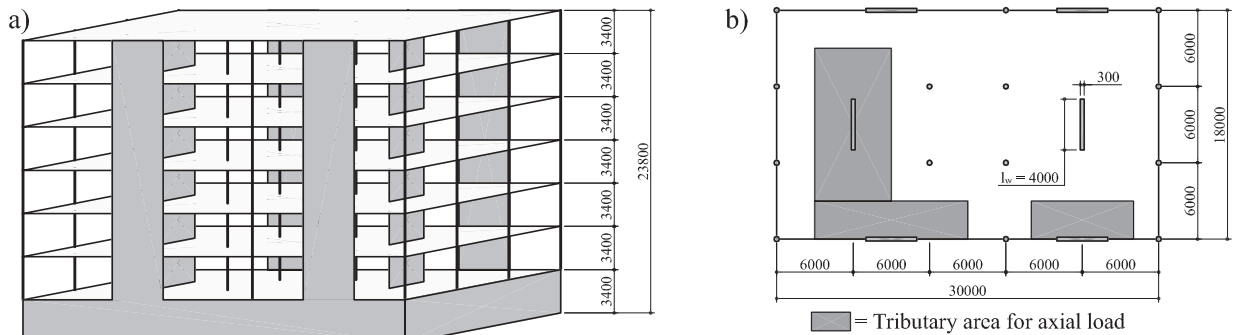


Figure 1: Reinforced concrete structural walls building (a) and relevant floor plan (b).

STATIC CYCLIC TESTS ON REINFORCED CONCRETE STRUCTURAL WALLS

The six units tested by Dazio and presented in [1] represent the lower part of the reinforced concrete structural walls of the six story reference building shown in Figure 1 at 50% scale. The test setup pictured in Figure 2a reproduced the same sectional forces in the plastic region of the test unit as in the structural walls of the reference building under seismic action.

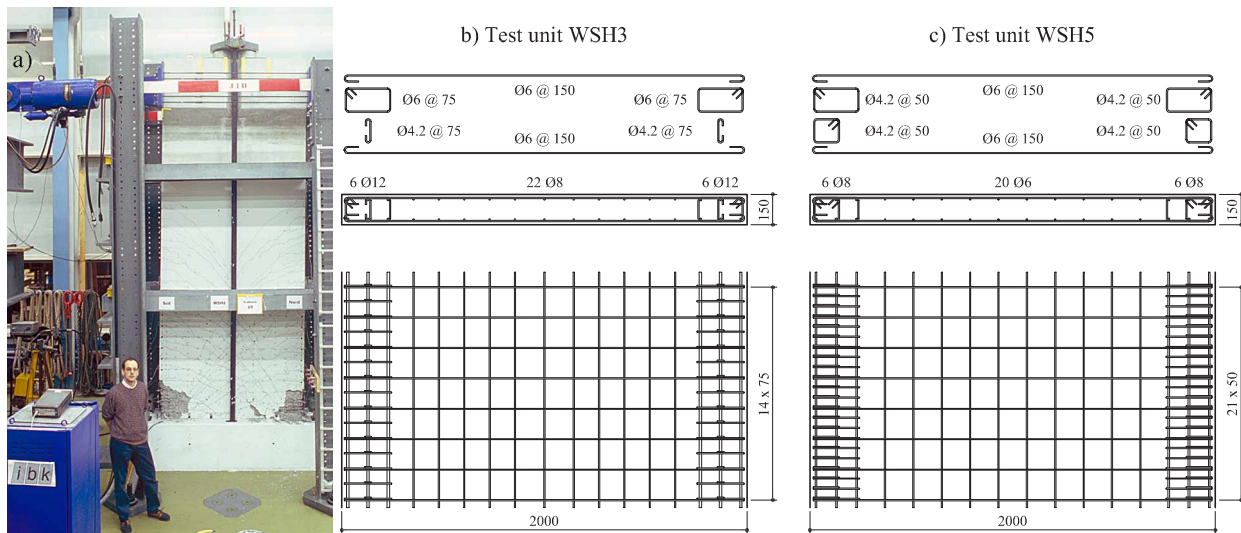


Figure 2: Setup for static cyclic tests of RC structural walls (a). Reinforcement of test units WSH3 (b) and WSH5 (c).

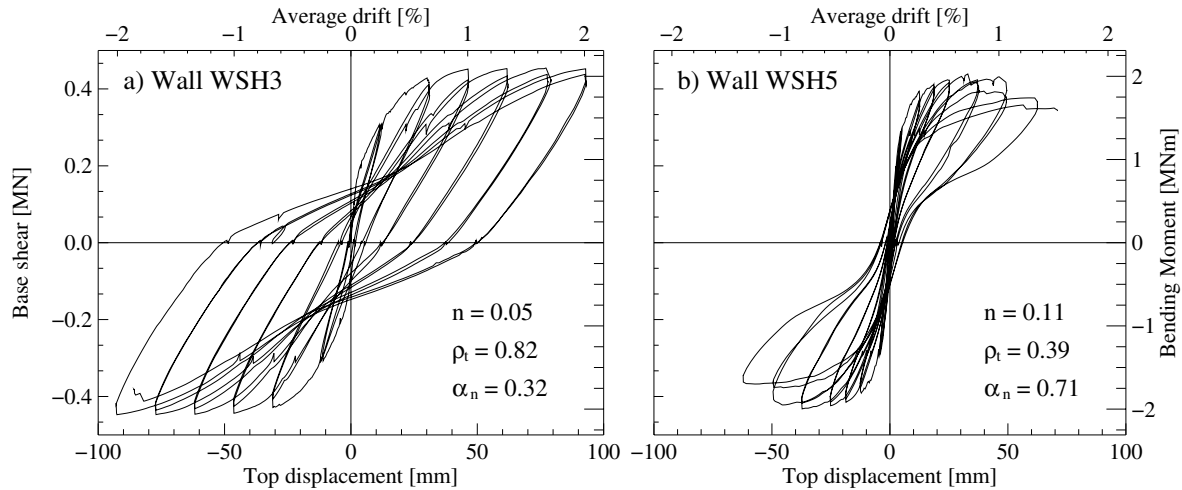


Figure 3: Hysteretic behavior of test units WSH3 (a) and WSH5 (b) [1].

The test matrix included variation of the ductility of the reinforcing steel, the longitudinal reinforcement ratio, the axial load ratio and the design method among the test units. A detailed discussion of all the test results is beyond the scope of this paper and only a comparison between the hysteretic behavior of the test units WSH3 and WSH5 is given here. Both walls had the same length l_w , hence almost the same yield displacement Δ_y . Figure 3 shows that also the bending strength of both walls was almost the same. In the case of wall WSH3 the bending strength was ensured by a total longitudinal reinforcement content $\rho_t = 0.82\%$ and an axial load ratio $n = N/(A_g f_c) = 0.05$. The same bending strength of wall WSH5 was ensured mainly by a high axial load ($n = 0.11$), because only the minimum reinforcement content was provided ($\rho_t = 0.39\%$). The reinforcement plan of both walls is pictured in Figures 2b and 2c.

Despite the similar monotonic behavior (same yield displacement and same bending strength) the two walls showed a fairly different hysteretic behavior:

- 1) The maximum residual displacement of wall WSH3 upon unloading was significantly larger. Even considering shake down effects, it is expected wall WSH3 to experience larger residual displacements after an earthquake, leading to a poorer performance.
- 2) The initial stiffness of both walls was similar. However, after plastic deformations occurred, the reloading stiffness of wall WSH5 was significantly larger because the high axial load was able to almost fully close flexural cracks during load reversal. Such a characteristic means that after an earthquake cracks are closed and do not need any repair. Furthermore, almost the entire initial stiffness of the wall is available, ensuring for example full serviceability for wind action.
- 3) Energy dissipation occurs mainly due to yielding of the reinforcement. Wall WSH3 had a larger reinforcement content and was able to dissipate 67% of the input energy while wall WSH5 could only dissipate 45% of the input energy. Therefore, the hysteresis curve of Wall WSH5 is characterized by a lower equivalent viscous damping, what according to modern design methodologies leads to larger displacement demands.
- 4) Because of the higher reinforcement content, wall WSH3 showed a higher post-yield stiffness that yielded to a larger plastic hinge length, hence a larger displacement capacity. However, in this particular case, wall WSH5 experienced a significantly lower displacement capacity mainly because of the poor material properties of the D6 web longitudinal reinforcement (see Figure 2).

Wall with bending strength due mostly to high axial load have significant advantages in terms of residual displacements and residual stiffness after an earthquake; two key parameters in the performance assessment of structures. However, the reduced energy dissipation capacity could lead to an increased displacement ductility demand. This issue is investigated in the following sections by means of finite element analyses.

SOFTWARE

To perform all numerical simulations presented in the next sections two different programs were implemented. In the followings they will be briefly presented.

The Takeda single degree of freedom (SDOF) system

The Takeda rules implemented to describe the hysteretic behavior of reinforced concrete structures are pictured in Figure 4 and correspond to the ones proposed in [4]. While the rules for cycles with large amplitude, Figure 4a, were derived from observations made during tests, the rules for small amplitude cycles are based mainly on engineering judgment and are set up to avoid clearly unrealistic behaviors during small cycles, i.e. to avoid very large or even negative reloading stiffnesses. Recognizing that the hysteretic rules assumed for the small amplitude cycles play an important role in the computation of the residual displacement it is important to always specify which rules are assumed for the analyses.

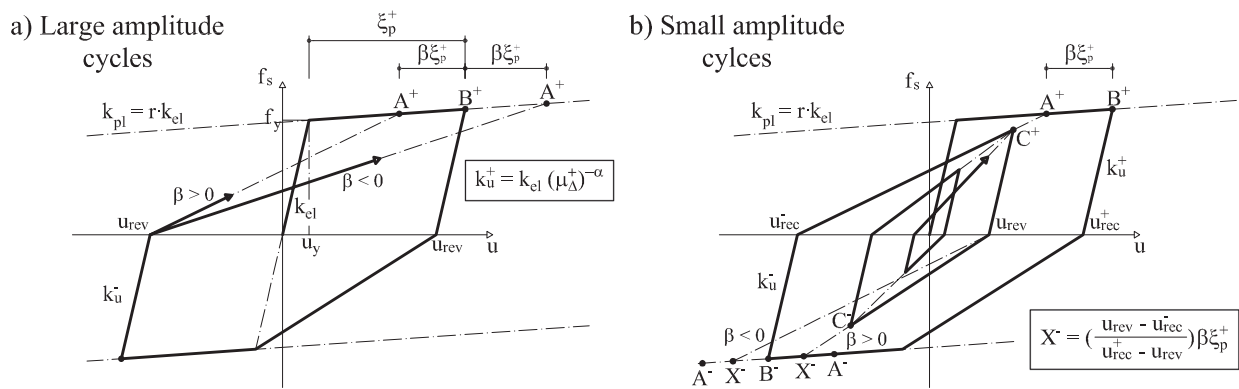


Figure 4: Hysteretic rules of the Takeda SDOF system: large amplitude cycles (a) and small amplitude cycles (b).

The fiber element program “Rechenbrett 2D”

“Rechenbrett-2D” is a simple program developed by Dazio [5] that allows the modeling of reinforced concrete structures with two-nodes Bernoulli beam fibre elements. This kind of elements are equivalent to a sectional analysis program performing moment curvature analysis, integrating curvatures along the element length and automatically accounting for the interaction between moment and axial load.

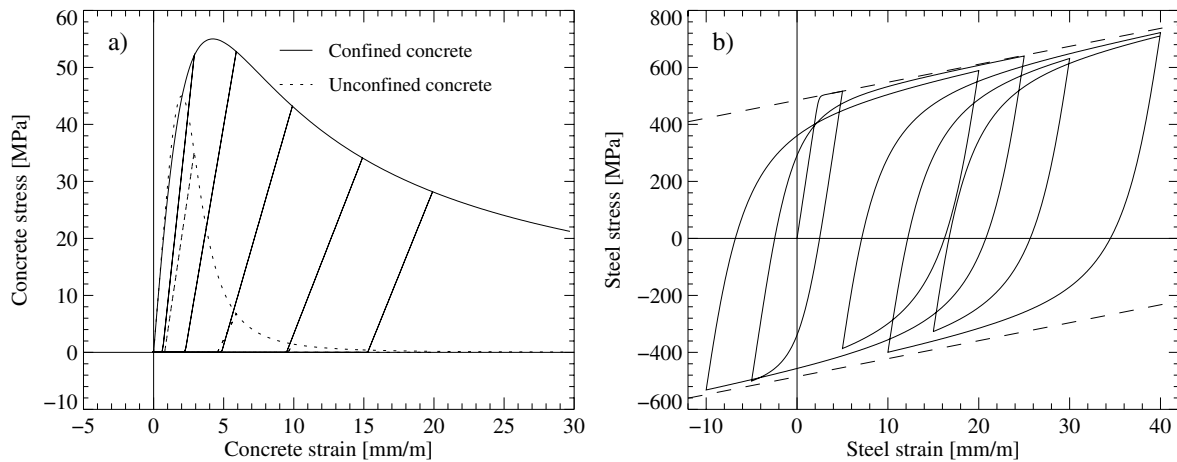


Figure 5: Simplified constitutive laws for concrete (a) and reinforcing steel (b).

The simplified uniaxial cyclic constitutive laws for reinforcing steel and concrete used by the elements are pictured in Figure 5 to allow a better interpretation of the results of the numerical simulations. The concrete constitutive law is a simplified version of the well known Mander's model, in which no tensile strength of the concrete is considered and where small unloading and reloading cycles occur with no energy dissipation as shown in Figure 5a. The also well known Menegotto-Pinto's steel constitutive law is pictured in Figure 5b. It allows a fairly accurate description of the Baushinger's effect, while no buckling of the longitudinal reinforcement is considered.

To ensure a good degree of robustness and to allow the computation of time history analyses, the constitutive laws for the materials were kept as simply as possible. Despite these simplifications, "Rechenbrett 2D" was able to predict fairly accurately the dynamic behavior of a 3-story reinforced concrete wall tested by Lestuzzi [2] on the ETH shake-table. The time history of the relative displacement of the wall is pictured in Figure 6a. The location of the amplitude maxima and their magnitude is well predicted. Discrepancies between test and simulation occurs in the free vibration phase at the end of the earthquake ($t > 10s$) mainly because in the test a friction damping occurred while in the simulation a viscous damping of the same magnitude was considered. The residual displacement predicted by the model is smaller than the measured one. Figures 6a and 6b show the measured and the computed cyclic moment-curvature relationship at the base of the wall. While the magnitude of moments and the curvatures is in good agreement, the shape of the reloading branches is different. Due to the presence of rough cracks the reloading stiffness of the test unit is smoother compared to the numerical simulation where a sharp bent can be observed when the "smooth cracks" of the model suddenly close shortly past the zero-curvature line and the stiffness rapidly increases.

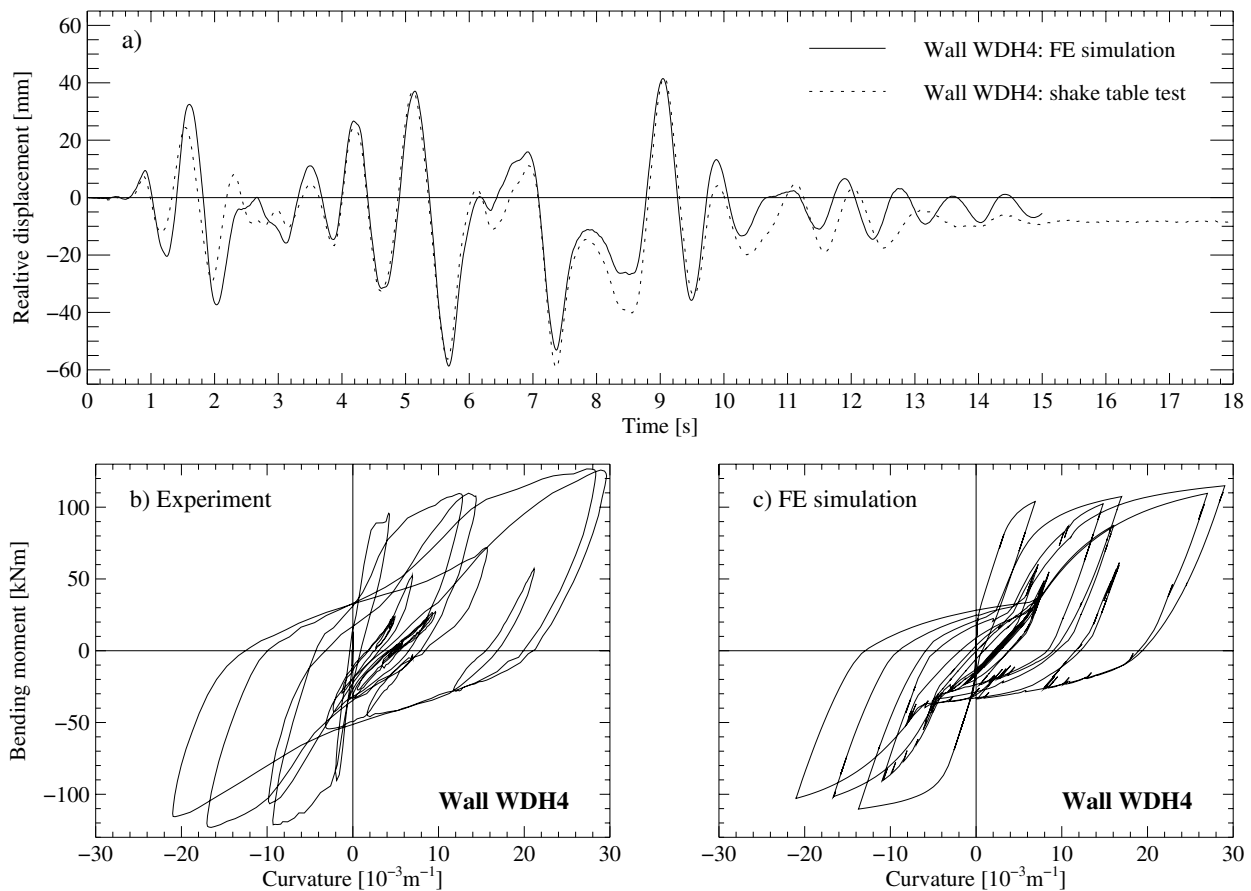


Figure 6: Simulation of the dynamic behavior of the wall WDH4 [2]. Time history of the top displacement (a) and cyclic moment-curvature relationships at the base of the wall (b, c).

ANALYSES

Chosen walls

To characterize reinforced concrete wall with different axial loads and different longitudinal reinforcement contents a new parameter α_n is introduced. α_n quantifies what part of the total bending strength of a wall is ensured by the axial load:

$$\alpha_n = \frac{0.45 \cdot l_w \cdot N}{M_n} \quad (1)$$

The numerator of Equation (1), where N is the axial load of the wall and l_w its length, is a good approximation for the contribution of the axial load to the nominal bending strength of the wall M_n . α_n is zero when there is no axial load and about one when there is no longitudinal reinforcement.

To investigate the influence of α_n on the behavior of reinforced concrete walls, a parametric study using eleven walls listed in Table 1 was carried out. The walls were all 4.0m long and 0.3m wide. The cylinder strength of the concrete was $f'_c = 40MPa$ and the yield strength of steel $f_y = 500MPa$ with hardening $b = 0.008$ typical of European Tempcore steels. All the walls had the same bending strength $M_n = 15MNm$. Walls N2 to N8 showed axial load ratios and reinforcement contents that can be found in real building, while walls N0, N1, N9 and N10 represented too extreme combinations of these parameters. Therefore, they were not further considered in parametric study.

Wall	M_n [kNm]	α_n [-]	N [kN]	n [-]	α_x [-]	ρ_t [-]	ρ_w [-]	ρ_e [-]	A_{se} [mm ²]	A_{sw} [mm ² /m]
N0	15000	0.00	0	0.000	0.037	0.0137	0.025	0.0585	7023	750
N1	15000	0.10	833	0.017	0.060	0.0123	0.025	0.0515	6183	750
N2	15000	0.20	1667	0.035	0.083	0.0110	0.025	0.0448	5379	750
N3	15000	0.30	2500	0.052	0.106	0.0097	0.025	0.0384	4611	750
N4	15000	0.40	3333	0.069	0.129	0.0085	0.025	0.0323	3879	750
N5	15000	0.50	4167	0.087	0.152	0.0073	0.025	0.0265	3183	750
N6	15000	0.60	5000	0.104	0.176	0.0062	0.025	0.0210	2524	750
N7	15000	0.70	5833	0.122	0.199	0.0052	0.025	0.0158	1900	750
N8	15000	0.80	6667	0.139	0.222	0.0042	0.025	0.0109	1313	750
N9	15000	0.90	7500	0.156	0.245	0.0033	0.025	0.0063	761	750
N10	15000	1.00	8333	0.174	0.268	0.0024	0.025	0.0021	246	750

Table 1: Eleven walls with the same bending strength given by different combinations of axial load and longitudinal reinforcement. (α_x = relative depth of the neutral axis, ρ_t , ρ_w , ρ_e = longitudinal reinforcement content of the wall, of the web region and of the end region, A_{se} , A_{sw} = steel area of the end and web regions of the wall).

Moment curvature analyses

Moment curvature diagrams for walls N2 to N8 are pictured in Figure 7 showing the dependence of the post-yield hardening on longitudinal reinforcement content. The nominal yield curvature was almost the same for all walls and corresponded to $\phi_y = 1 \cdot 10^{-3} m^{-1}$. Figure 7b shows that up to nominal yield the secant stiffness of the walls is influenced by the axial load and that the tangent stiffness is highly nonlinear already in elastic region of the moment curvature diagram.

The assumed steel properties led to a post-yield stiffness of the walls ranging between 0.3 and 1.0% of the elastic stiffness, i.e. very low. Assuming a hardening $b = 0.013$ of the reinforcement - corresponding to typical US Grade 60 steel - the post-yield stiffness ranges between 0.5 and 1.5% of the elastic stiffness.

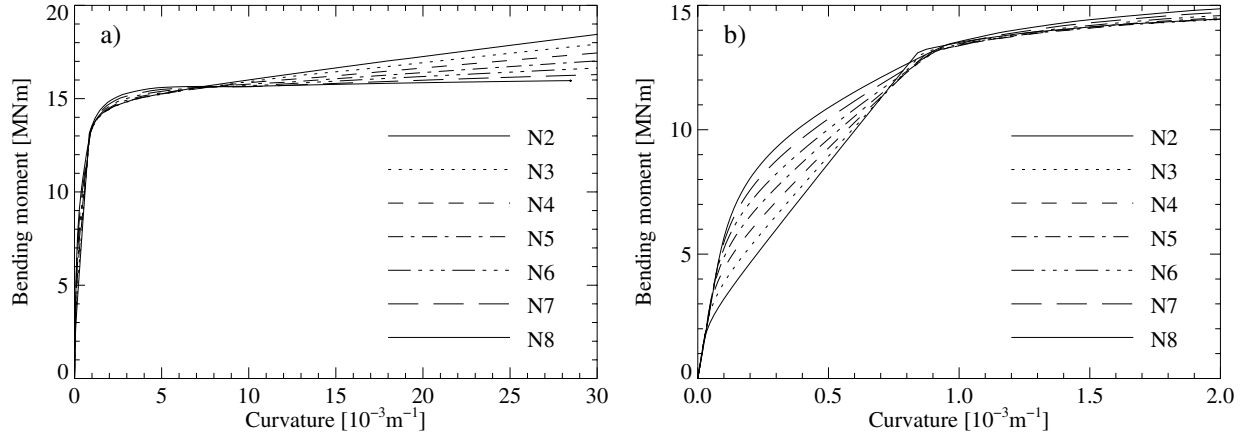


Figure 7: Moment-curvature relationship of the seven walls N2 to N8 (a). Magnified view of the elastic region (b).

Static cyclic analyses

The energy dissipation capacity of the different walls and its influence on the dynamic behavior of the latter was first analyzed by means of static cyclic numerical analyses. Single degree of freedom (SDOF) systems equivalent to the 4-DOF system shown in Figure 10b were implemented in “Rechenbrett 2D” and static cyclic analyses were performed using a conventional loading history with symmetric cycles of increasing amplitude. The hysteretic behavior of the walls N2, N5 and N7 is pictured in Figures 8a to 8c. The influence of the parameter α_n on the hysteretic behavior is evident and confirms the experimental observations presented in the previous sections. “Rechenbrett 2D” does not take into account shear deformations. Therefore, the pinching in the hysteresis loops is due to the axial load alone. Pinching means reduced energy dissipation capacity and while in correspondence of displacement ductility $\mu_\Delta = 6$ wall N2 was able to dissipate 80% of the input energy, wall N7 dissipated just 45% of it.

The equivalent viscous damping ζ_{eq} is also an indicator of energy dissipation capacity and is plotted for all walls in Figure 8d. The dotted line is a proposal by Priestley [6] to estimate the equivalent viscous damping of reinforced concrete walls. The proposal corresponds basically to the average value of all computed cases. However, it does not consider the dependency between ζ_{eq} and α_n . According to modern design methodologies, a lower value of ζ_{eq} leads to larger displacement demands. This increase in displacement demand can be estimated by means of Equation (2) where S_{d1} is the spectral displacement of a SDOF system of period T_n and damping ζ_1 .

$$\frac{S_{d1}(T_n, \zeta_1)}{S_{d2}(T_n, \zeta_2)} = \sqrt{\frac{2 + \zeta_2}{2 + \zeta_1}} \quad (2)$$

Let be wall N2 designed using direct displacement design principles for a target displacement ductility $\mu_\Delta = 2$, then wall N7 - designed to have the same monotonic behavior as N2 (neglecting the fact that by identical target displacement the secant stiff of wall N7 would be slightly smaller than wall N2) - would reach a displacement ductility $\mu_\Delta = 2.4$. In the same way it can be shown that when wall N2 is designed for a target displacement ductility $\mu_\Delta = 5$, wall N7 would reach $\mu_\Delta = 6.6$. The equivalent viscous damping ζ_{eq} plotted in Figure 8d considers hysteretic damping only. However, to compute the target displacements of walls N2 and N7 an additional 5% damping to account for system damping was used. Considering that the design ductility of a structure seldom exceeds 4 because of serviceability and performance considerations, the assumption of an average equivalent viscous damping value independent from α_n for all wall types seems reasonable. Such an assumption leads theoretically to differences in the estimated displacement demand of the order of 10%, what is small compared to the uncertainties related to the seismic action. However, in the following sections, this issue will be investigated by means of transient analyses.

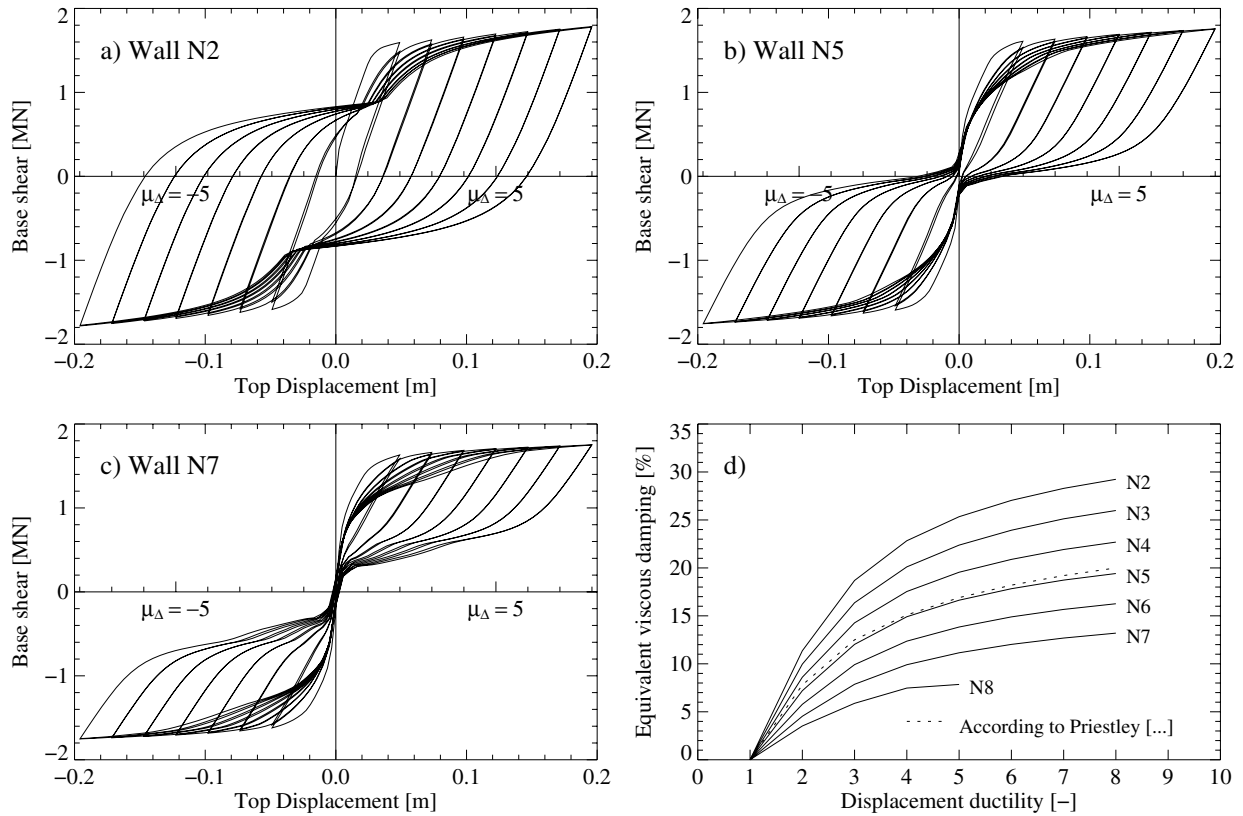


Figure 8: Force-displacement relationship of walls N2, N5, N7 (a-c) and relevant equivalent viscous damping (d).

Ground Motions

In the following section time history analyses are performed using 5 different ground motions. The response spectra of these ground motions are pictured in Figure 9 for a viscous damping $\zeta = 5\%$. The different ground motions were scaled using different factors ranging from 0.20 to 4.63 depending on the target displacement ductility assumed for each computation.

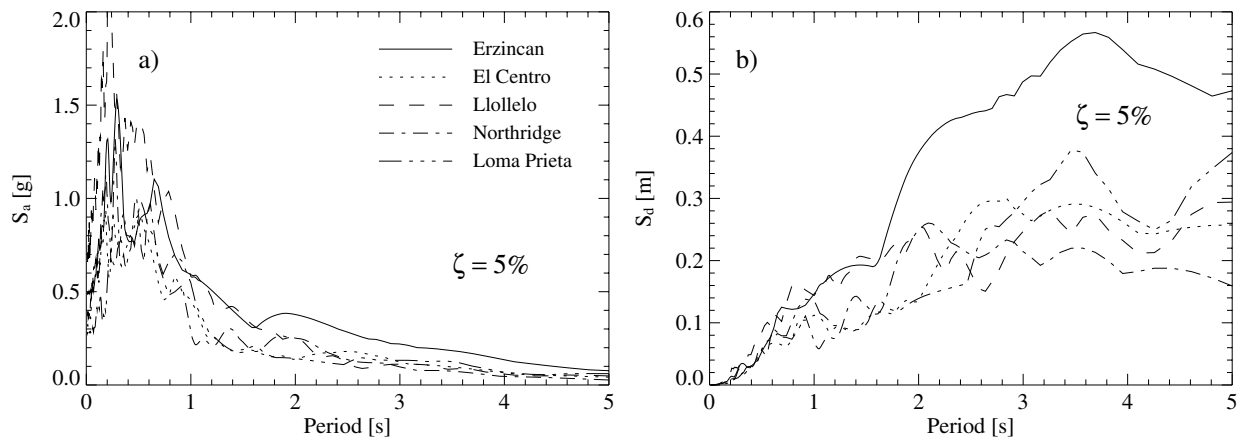


Figure 9: Acceleration (a) and displacement (b) response spectra of the ground motions considered in the time history analyses.

Dynamic analyses on multi degrees of freedom systems

The dynamic behavior of multistory walls is investigated by means of time-history analysis. Totally 480 cases given by permutation of 2 dynamic systems (4-DOF and 7-DOF), 3 effective natural periods (0.61, 0.91 and 1.82 seconds), 2 reinforcing steel hardening ratios b (0.008 and 0.013), 2 target displacement ductilities μ_{Δ} (2.5 and 4.5) and 5 ground motions were analyzed.

The elevation of the considered dynamic systems is pictured in Figures 10a and 10b; each story has the same mass and its magnitude is calculated in function of the target period of the system. The axial load generated by each story is the same and the total axial load in the plastic hinge region of each wall is given in Table 1. The discretization of the section and the relevant material properties are given in Figure 10c. The ground motions pictured in Figure 9 were scaled by means of the equal displacement principle so that the wall would reach the targeted displacement ductility.

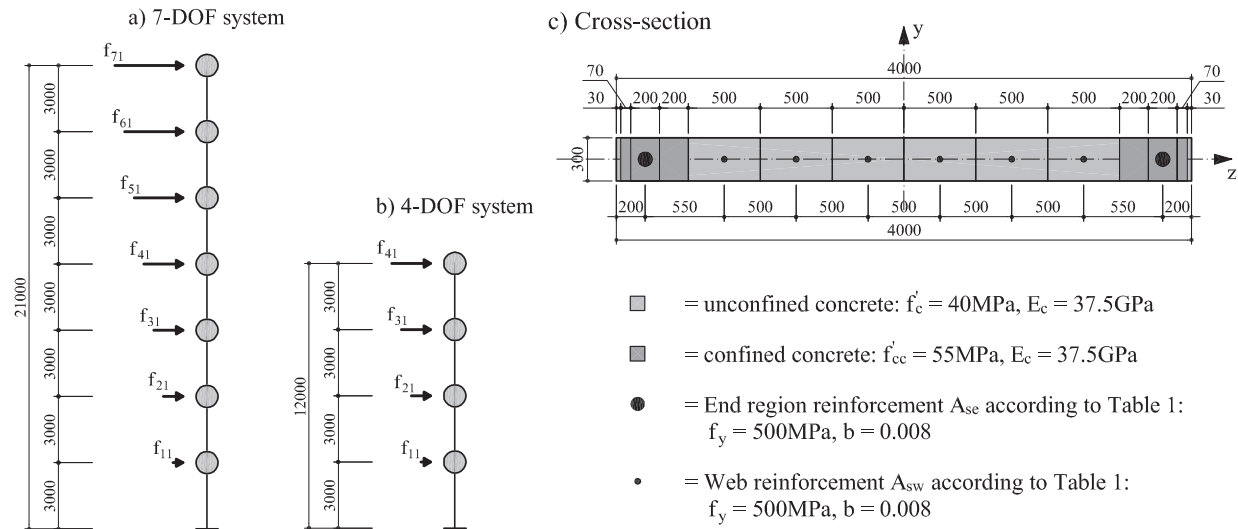


Figure 10: Dynamic systems (a, b) and typical cross-section with relevant material properties (c).

Among all the results produced by the analyses, here only the ones relevant to maximum ductility demand and residual displacement are displayed in Figure 11. The computations performed on the 7-DOF system produced basically the same results as for the 4-DOF system. Therefore, only the latter will be further discussed. In the case of target ductility $\mu_{\Delta} = 2.5$, wall N2 reached an average ductility of 2.20 while the average value for wall N8 was 2.43, i.e. an increase of 10%. For a target ductility of $\mu_{\Delta} = 4.5$ the same values were 4.33, 4.96 and 15%, respectively. The scatter is similar to the one predicted using the equivalent viscous damping approach presented before. These results confirm previous investigation performed by Dazio [5] and is in excellent agreement with the results obtained by Christopoulos and co-workers while analyzing the displacement demand of flag-shaped hysteretic models [7, 8, 9]. Furthermore, in [5] it is shown that significantly higher ductility demands - in the order of about 30 to 40% - for walls with higher axial load occur only when a target ductility of $\mu_{\Delta} = 6.5$ or higher is assumed. However, it is very unlikely that a real structure would be designed for such a large target ductility, therefore the meaning of this last finding is of relative importance.

Figure 11c displays the ratio between the residual displacement of the wall at the end of the time history to the maximum displacement reached by the wall during the same time history. The target displacement ductility, i.e. the maximum displacement reached by the wall, had little influence on the ratio. The same finding was reported in [7]. On the other hand and as expected, the ratio is inversely proportional to the parameter α_n . It has to be noted that the magnitude of the ratio resulting from these computation is, especially for wall with low axial load, somewhat smaller compared to the results obtained by other researchers. This effect is probably due to the shape of the reloading branches produced by the fiber

model. The sudden closure of the smooth cracks and the relatively high reloading stiffness of the concrete material model (see Figure 5a) generates reloading branches starting with low stiffness that suddenly increases just past zero horizontal displacement. This creates a kind of artificial self-centering mechanism that in real reinforced concrete elements is also present, however, it is not so pronounced. This example shows the importance of the definition of the hysteretic rules for small amplitude cycles.

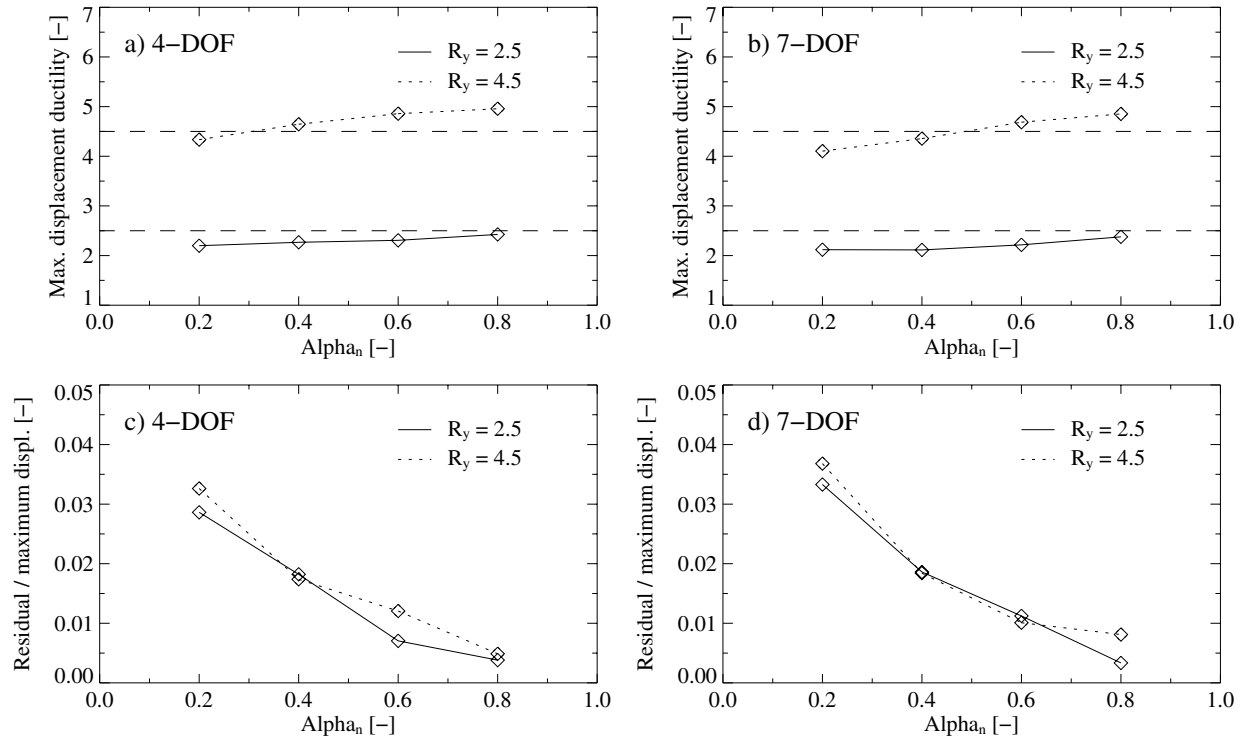


Figure 11: Average maximum displacement ductility (a, b) and average relative residual displacement (c, d) in function of the parameter α_n .

Dynamic analyses on single degree of freedom systems

The dynamic behavior of ductile reinforced concrete walls was further investigated by means of nonlinear SDOF systems. Due to the significantly smaller computational burden it was possible to run a higher number of cases as in the previous section. Totally 14400 cases given by permutation of 4 natural periods (0.61, 0.91, 1.82 and 3.64 seconds), 3 hardening ratios r (0, 5 and 10%), 5 Takeda α -parameters (0.0, 0.2, 0.4, 0.6 and 0.8), 6 Takeda β -parameters (0.0, 0.2, 0.4, 0.6 and 0.8), 2 target ductilities μ_Δ (2.5 and 4.5) and 20 ground motions were analyzed.

Before the results on the analyses are presented, a brief comment on the shape of small amplitude cycles of SDOF systems is due. Figure 12 shows on the top the time history of 3 Takeda-type SDOF systems with the same monotonic backbone curve, the same unloading stiffness factor α but different reloading stiffness factors β . Each one of these time histories is compared with the time history of a SDOF system with the same monotonic backbone curve but modeled with “Rechenbrett 2D” (dotted line). On the bottom of Figure 12, the hysteresis loops of the same SDOF systems are pictured.

For the computation plotted in Figure 12a, a Takeda $\beta = 0.0$ and the hysteresis rules on Figure 4 were used. While the comparison of the large amplitude cycles between the two SDOF systems is excellent (up to the fourth large peak), the reloading stiffness of the Takeda model is significantly lower leading to quite

different small amplitude cycles and residual displacements. For the computation plotted in Figure 12b, a Takeda $\beta=0.9$ and the hysteresis rules on Figure 4 were used. While the magnitude of the large amplitude cycles between the two SDOF systems is very similar up to the third large peak, the comparison of the reloading branches of the large amplitude cycles are not very good. On the other hand the small cycle behavior of the two SDOF systems is very similar and the residual displacements correspond. For the computation plotted in Figure 12c, a Takeda model with $\beta=0.9$ for large amplitude cycles and $\beta=0.0$ for small amplitude cycles was used. This shows the importance of the definition of small amplitudes cycles on residual displacements. While the large cycle response of the Takeda SDOF systems in Figures 12b and 12c are coincident, the small cycles are completely different leading also to completely different residual displacements.

Figure 13 is similar to Figure 11. In both cases the residual displacement ratio and the maximum displacement ductility are plotted against a parameter that strongly affects the unloading stiffness of the hysteresis loops and the results show the same trends. A typical reinforced concrete structure can be modeled using the Takeda parameter $\alpha=0.2$ and $\beta=0.4$. According to Figure 13a, the average residual displacement ratio for such SDOF systems is about 0.085. Changing β from 0.4 to -0.2 would increase the average residual displacement ratio by a factor 1.8 and changing α from 0.2 to 0.6 would decrease the average residual displacement ratio by a factor 2.8. The influence of both Takeda parameters on residual displacements is therefore significant. On the other hand, Figure 13b shows that both parameters have a limited influence on the maximum displacement ductility like it was the case in Figure 11. It has to be noted that in Figure 13 for sake of completeness all the combinations of the Takeda parameters α and β are plotted. However, when both parameters are large and specially when the hardening parameter $r=10\%$ is used, odd hysteresis loops can results and the interpretation of the results has to be carried out with caution. In a similar study presented in [7] the same conclusions regarding the influence of the parameter Takeda β on residual deformations were drawn. However, in that study the parameter Takeda α had a smaller influence on residual deformations has it has here.

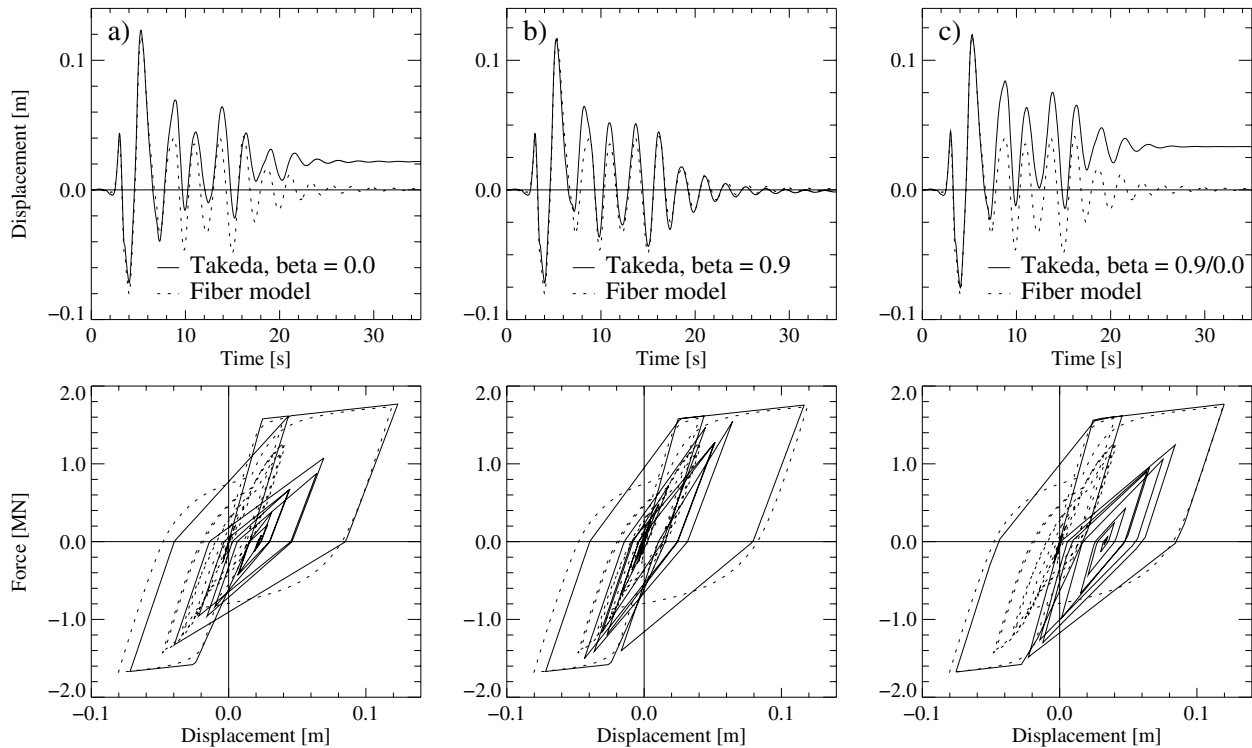


Figure 12: Influence of the Takeda small-cycles hysteresis rules on the residual displacement of single degree of freedom systems.

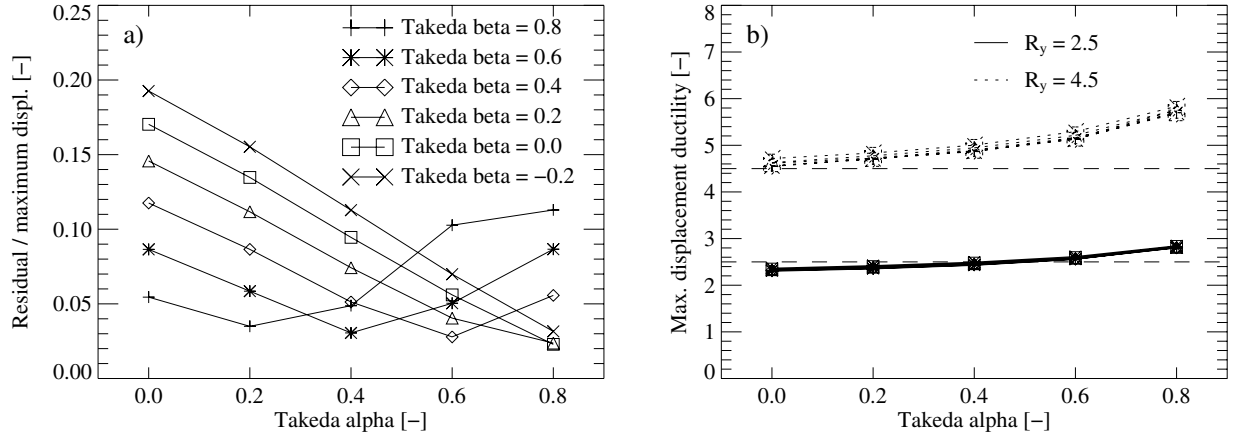


Figure 13: Influence of the Takeda parameters α and β on the relative residual displacements (a) and on the ductility demand (b) of single degree of freedom systems.

RECCOMENDATIONS

It was shown that walls with bending strength due mostly to high axial load have significant advantages in terms of residual displacements and residual stiffness after an earthquake; while the reduced energy dissipation capacity has in most practical cases negligible effects. Therefore, a structure should be designed targeting walls with α_n as large as possible. To reach this goal, the tributary area of the walls can be increased by increasing the span of the slabs or by choosing an appropriate location of the wall within the floor plan (see Figure 1). However, even if not specifically investigated in this paper, it has to be noted that walls with a high value of α_n develop a reduced plastic hinge length leading to a lower maximum displacement capacity. Therefore the value of α_n should be limited to:

$$\alpha_n \leq 0.70 \quad (3)$$

or to:

$$\alpha_n \leq 1.35 \frac{n}{n + (0.75 / \sqrt{f'_c})} \quad (4)$$

whichever is smaller. In Equation (4) $n = N / (A_g f'_c)$ is the axial load ratio of the wall and f'_c is the cylinder strength of the concrete. The limit given by Equation (4) ensures that the nominal bending strength of the wall is at least twice the cracking moment of the wall as recommended by Priestley in [9].

PERMANENT DISPLACEMENT OF A BRIDGE PIER: AN EXAMPLE

In the framework of the proof testing in support to the design of the new East Spans of the San Francisco-Oakland Bay Bridge performed in the laboratories of the University of California, San Diego; a quarter scale model of the West Anchor Pier (Pier W2) of the Main Span Self-anchored Suspension Bridge was tested by Seible and Dazio [10, 11]. Two of the eight column forming Pier W2 were modeled in the laboratory and tested using the setup pictured in Figure 14a. The test unit showed an excellent hysteretic behavior (Figure 14b) and could easily outperform all the performance criteria required by the design specification. A computation by means of “Rechenbrett 2D” was able to predict the global behavior of the test unit fairly accurately, while being able to exactly predict the permanent deformations.

During the so-called Safety Evaluation Earthquake (SEE), Pier W2 is expected to undergo plastic deformations up to a displacement ductility of about two. Upon unloading after such a displacement, the maximum possible residual displacement of the stand-alone Pier W2 measured during the test was

100mm, corresponding to 400mm in the prototype structure. This value does not conform with the performance requirement limiting permanent deformations to 300mm. Time history analyses of the bridge under the SEE Event showed that taking into account shake-down effects, the expected residual displacement is well below the permitted limit. However, considering that the maximum displacement capacity of the Pier was not an issue being more than three times larger than the seismic demand, this example shows that residual displacements are important design parameters for ductile bridge piers.

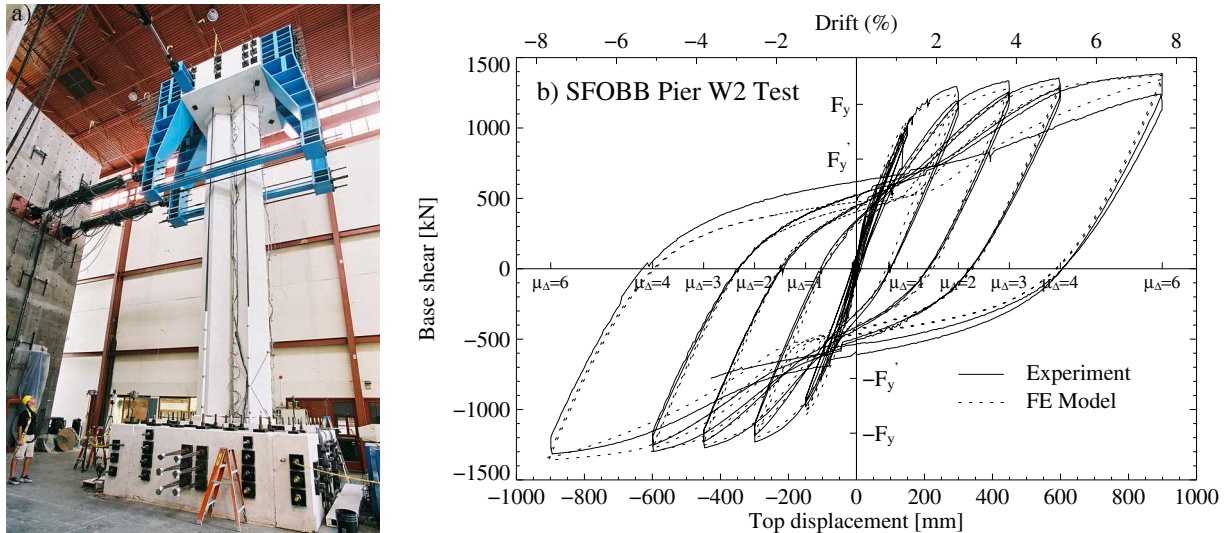


Figure 14: Setup for Pier W2 Test (a). Measured and predicted hysteretic behavior of the test unit (b).

In the previous sections it was shown that increasing the axial load will reduce the maximum possible residual displacement of reinforced concrete elements. In the followings, the influence of the shape of bridge piers on permanent deformations is investigated. Figure 15a shows the cross-section of the unit tested in the laboratories. The two circular columns had a diameter of 0.88m and a clear height of 10.5m. The columns were fixed at the base, separated by a 127mm gap along the height and connected at the top by a rigid cap beam. To ensure visual consistency with the rest of the prototype bridge, the columns were provided with a pentagonal shaped architectural concrete. Figures 15b and 15c show design alternatives of the test unit. The circular section and the hollow section were designed in such a way that the corresponding Pier would have an almost identical monotonic behavior as the Test Unit, assuming that the acting axial load was the same on the three piers (See Figure 16a).

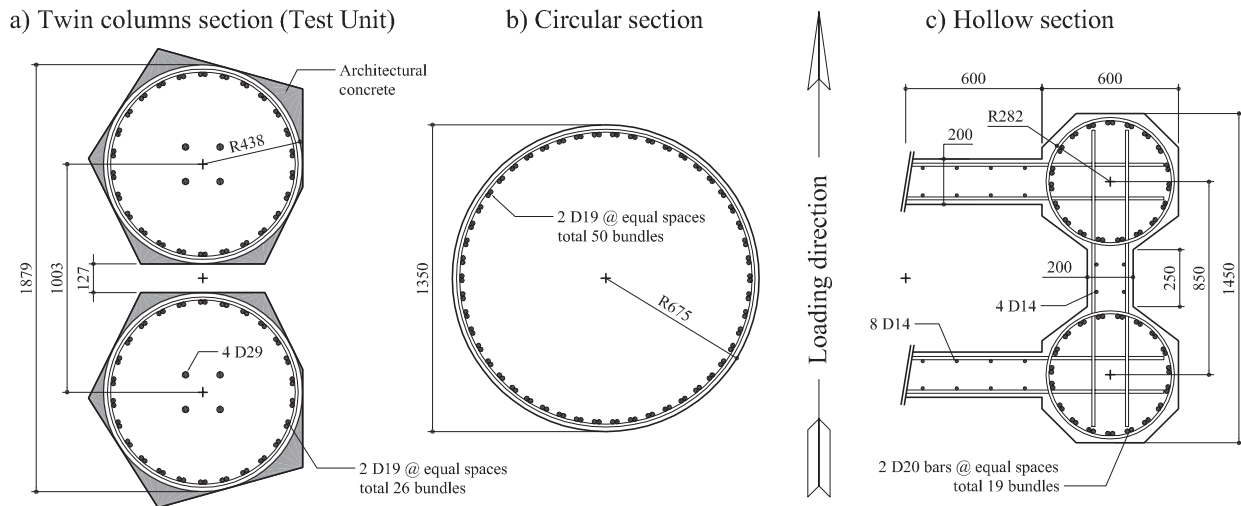


Figure 15: Design alternatives of the Pier W2 Test Unit.

The three piers were modeled with “Rechenbrett 2D” and subjected to the same loading as the Pier W2 Test Unit during the laboratory testing. Figure 16b shows the computed hysteretic behavior and while the reloading stiffness of the three piers is similar, the unloading stiffness of the piers with circular and hollow sections is larger leading to larger maximum possible residual deformations. Upon unloading from a displacement ductility of two, the residual deformation of the latter piers was 140mm, i.e. 40% larger than the one of the test unit.

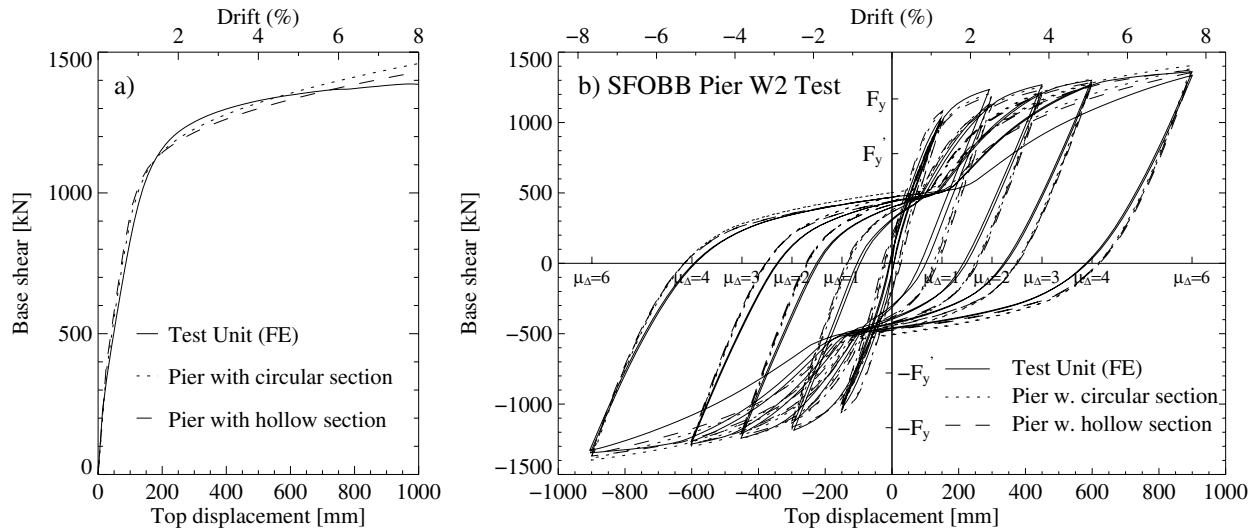


Figure 16: Predicted monotonic (a) and cyclic (b) behavior of the three design alternatives of Pier W2 Test Unit.

CONCLUSIONS

Walls with bending strength due mostly to high axial load are characterized by a large value of the newly defined moment ratio α_n . Hysteresis loops generated using large values of α_n are almost flag-shaped ensuring self-centering properties of such walls. The dynamic behavior of flag-shaped hysteretic models has already been investigated and researchers report that despite the limited energy dissipation capacity of this type of inelastic oscillators, their maximum displacement ductility demand is only slightly larger compared to systems with larger equivalent viscous damping. These findings were confirmed by the analyses presented in this paper.

Post-tensioned precast walls have a value of α_n close to unity and perform extremely well under seismic action. In capacity designed walls the value of α_n has to be limited to prevent a premature failure of the longitudinal reinforcement. Suggested limits for α_n are given in the relevant section of the paper.

Time history analyses showed that maximum displacements of RC structures subjected to earthquake are rather insensitive to the shape of the hysteresis loops, provided the monotonic backbone curve is the same. On the other hand, residual displacements are very sensitive to the shape of the hysteresis loops. Therefore, hysteresis rules for small amplitude cycles have to be carefully chosen. Fiber models are very suitable to predict the behavior of structures, however, to correctly deal with residual deformations the constitutive laws of the concrete should properly take into account cracking. The constitutive laws of the steel should properly take into account the Bauschinger's effect.

In cases where it is not appropriate to increase the axial load, a reduction of the permanent displacement potential can be achieved by optimizing the shape of the element's cross section. Twin column or twin wall sections seem to provide a reduction of permanent displacement, this because of the additional axial load due to frame action between the columns or the walls.

AKNOWLEDGEMENTS

The author is highly indebted to Professor Dr. Dr h.c. Hugo Bachmann, Professor Emeritus, Institute of Structural Engineering (IBK), Swiss Federal Institute of Technology (ETH), Zurich, and to Professor Dr. Frieder Seible, Dean Jacobs School of Engineering, University of California San Diego (UCSD) for the support and guidance provided to the author during his stay at the respective Institutions.

REFERENCES

1. Dazio A, Wenk Th, Bachmann H. „Versuche an Stahlbetontragwänden unter zyklisch-statischer Einwirkung. (Tests on RC Structural Walls under Cyclic-Static Action)”. IBK-ETH Zurich. IBK-Report No. 239, ISBN 3-7643-6149-2. Birkhäuser Verlag, Basel 1999.
2. Lestuzzi P, Wenk Th, Bachmann H. “Dynamische Versuche an Stahlbetontragwänden auf dem ETH-Erdbebensimulator. (Dynamic Tests on RC Structural Walls on the ETH Shaking Table)”. IBK-ETH Zurich. IBK-Report No. 240, ISBN 3-7643-6162-X. Birkhäuser Verlag, Basel 1999.
3. Thiele K, Wenk Th, Bachmann H. “Versuche an Stahlbetontragwänden unter pseudodynamischer Einwirkung. (Pseudo-Dynamic Tests on RC Structural)”. IBK-ETH Zurich. IBK-Report No. 257, ISBN 3-7643-6526-9. Birkhäuser Verlag, Basel 2000.
4. Allahabadi R, Powell G. “Drain-2DX, User Guide”. Report UBC/EERC-88/06. Earthquake Engineering Research Center, University of California, Berkeley 1988.
5. Dazio A. „Entwurf und Bemessung von Tragwandgebäuden unter Erdbebeneinwirkung (Design and Detailing of RC-Wall Buildings under Seismic Action)“. IBK-ETH Zurich. IBK Report Nr. 254. ISBN 3-7643-6471-8. Birkhäuser Verlag, Basel 2000.
6. Priestley MJN. “Performance Based Seismic Design”. Proceedings of the XII World Conference on Earthquake Engineering, Auckland, New Zealand 30 January - 4 February 2000.
7. Christopoulos C, Pampanin S, Priestley MJN. “Performance-Based Seismic Response of Frame Structures Including Residual Deformations. Part I: Single-Degree of Freedom Systems”. Journal of Earthquake Engineering 2003; 7(1): 97-118.
8. Christopoulos C, Filiatrault A, Folz B. “Seismic response of self-centering hysteretic SDOF systems”. Earthquake Engineering and Structural Dynamics 2002, 31: 1131-1150
9. Pampanin S, Christopoulos C, Priestley MJN. “Performance-Based Seismic Response of Frame Structures Including Residual Deformations. Part II: Multi-Degree of Freedom Systems”. Journal of Earthquake Engineering 2003; 7(1): 119-147.
10. Priestley MJN, Seible F, Calvi GM. “Seismic Design and Retrofit of Bridges”. John Wiley & Sons, 1996
11. Dazio A, Seible F. “Structural Testing of the San Francisco-Oakland Bay Bridge Main Span Pier W2”. SSRP Report 2002/11. Department of Structural Engineering. University of California, San Diego. La Jolla, CA, 2002.
12. Seible F, Dazio A. “Proof Testing in Support of Seismic Bridge Design: Example of the San Francisco-Oakland East Bay Safety Project”. Proceeding of the FIB 2003 Symposium Concrete Structures in Seismic Regions. Athens May 6-9, 2003